ADAPTIVE COMPENSATION OF SENSOR RUNOUT FOR MAGNETIC BEARINGS WITH UNCERTAIN PARAMETERS: THEORY AND EXPERIMENTS

Joga D. Setiawan Ranjan Mukherjee
Department of Mechanical Engineering
Michigan State University
East Lansing, MI 48824-1226

Eric H. Maslen
Department of Mechanical and Aerospace Engineering
University of Virginia
Charlottesville, VA 22903

SUMMARY

The problem of sensor runout in magnetic bearing systems has been largely overlooked due to similarities with mass unbalance in creating periodic disturbances. While the effect of mass unbalance can be significantly reduced, if not eliminated, through rotor balancing, sensor runout disturbance is unavoidable since it originates from physical nonconcentricity between rotor and stator. Sensor runout is also caused by nonuniform electrical and magnetic properties around the sensing surface. To improve performance of magnetic bearings, we present an adaptive algorithm for sensor runout compensation. It guarantees asymptotic stability of the rotor geometric center and on-line feedforward cancellation of runout disturbances using persistent excitation. Some of the advantages of our algorithm include simplicity of design and implementation, stability, and robustness to plant parameter uncertainties. The stability and robustness properties are derived from passivity of the closed-loop system. Numerical simulations are presented to demonstrate efficacy of the algorithm and experimental results confirm stability and robustness for large variation in plant parameters.

I. INTRODUCTION

Active magnetic bearings have a number of advantages over conventional bearings. These advantages include elimination of lubrication system, friction free operation, operation capability at temperature extremes and at higher rpm, reduced power consumption, and adjustable stiffness and damping characteristics achieved through active control of bearing forces. The bearing forces are also used for cancelling periodic disturbances, which, common in rotating machinery, cause vibration, degrade performance, and sometimes lead to instability.

The dominant sources of periodic disturbance in magnetic bearings are mass unbalance and sensor runout. Mass unbalance results from lack of alignment between the geometric axis and the principal axis of inertia, and results in an unbalance force synchronous with rotor angular speed. Mass unbalance can be significantly reduced in industrial applications, if not completely eliminated, by rotor balancing. In comparison, sensor runout is unavoidable since it results from manufacturing imperfections in the magnetic bearing assembly. Specifically, sensor runout disturbance originates from lack of concentricity of the sensing surface, and non-uniform electrical

or magnetic properties around the sensing surface. Unlike mass unbalance, sensor runout also generates disturbance at multiple harmonics of angular speed. Despite differences between mass unbalance and sensor runout disturbances, the control objective for their compensation is often similar. Stabilization of the rotor about the geometric center, which is the objective for sensor runout compensation, is often the objective for unbalance compensation.

Though few researchers (Setiawan, et al., 1999) have addressed the problem of compensation of combined unbalance and sensor runout disturbances, there exists a large volume of research on compensation of individual disturbances. Some of the early work on unbalance compensation has been based on insertion of a notch filter in the control loop (Batty, 1988). The drawback of this approach stems from negative phase of the notch transfer function which can reduce stability margin of the closed-loop system and lead to instability (Knospe, 1991; Bleuler, et al., 1994; Na and Park, 1997). Another approach for periodic disturbance cancellation is adaptive feedforward control (Shafai, et al., 1994; Hu and Tomizuka, 1993), where fourier coefficients of the disturbance are continually estimated and used for cancellation. These adaptive controllers, operationally bear resemblence to the notch filters (Na and Park, 1997) and can result in instability, if designed without considering the underlying structure of the system. To preserve stability of the closed-loop system, Herzog, et al. (1996) developed the generalized notch filter and Na and Park (1997) proposed variation of the least mean square algorithm. For improved performance in disk drives, Sacks, et al. (1996) modified the feedforward controller to remove oscillations from the transient response for faster parameter convergence. Other approaches that compensate unbalance while ensuring stability include adaptive auto-centering (Lum, et al., 1996) and output regulation with internal stability (Matsumura, et al., 1990). Both these approaches achieve rotor stabilization about the center-of-mass.

Though unbalance compensation has been widely studied with the objective of stabilization about the mass center, most users and vendors push for geometric centering accepting that the real objective is to avoid seal or aero tip collisions. While geometric center stabilization has been addressed by a few researchers (Hisatani and Koizumi, 1994; Song and Mukherjee, 1996), both problems were investigated by Reinig and Desrochers (1986) and Mizuno and Higuchi (1990). These results indicate stabilization about mass center or geometric center can be achieved through cancellation of disturbance in the current signal or the displacement signal, respectively. In a general and experimental approach for disturbance attenuation (Knospe, et al., 1996; 1997), any form of rotor vibration that can be measured, can be attenuated using pseudo-inverse of the pre-computed influence coefficient matrix. The stability and performance of the algorithm in the presence of uncertainties were investigated, and experimental results were used to demonstrate effectiveness. The method decouples the problem into two independent control tasks, and while it has been demonstrated to work successfully, there is no theoretical basis for stability of the two interacting processes. Some of the other approaches employed for unbalance compensation include robust control designs (Fujita, et al., 1993; Rutland, et al., 1994), Q-parameterization control (Mohamed et al., 1997), and neural networks (Paul, et al., 1997).

In this paper we address the problem of sensor runout compensation with the objective of rotor stabilization about the geometric center. This problem was recently investigated by Kim and Lee (1997), where the open-loop influence coefficient method (Knospe, et al., 1997) was used to suppress vibration at the fundamental frequency and at higher harmonics. Our approach to the problem is based on traditional adaptive control designs (Narendra and Annaswamy, 1989)

that guarantee both plant stability and convergence of unknown parameters in the persistency of excitation. While such methods based on Lyapunov stability theory have found applications for stepper motors (Chen and Paden, 1993), they have not been used for the control of magnetic bearings. To this end we design a simple, yet robust, adaptive feedforward controller for rotor stabilization in the presence of sensor runout disturbances. The salient features of our controller include simplicity of design and implementation, closed-loop estimation and cancellation of sensor runout harmonics, asymptotic stability of the complete system, and robustness to significant variation in plant parameters. The robustness of our algorithm does not require separate control action; it is an artifact of passivity of the closed-loop system. Such inherent robustness provides advantages over state-space approaches based on deterministic models. In such approaches the disturbance harmonics are modeled using linear oscillators and estimated with an observer. In the presence of parameter uncertainty, asymptotic stability of the observer is not guaranteed .

This paper is organized as follows. The mathematical model of the magnetic bearing with sensor runout is presented in section II. The sensor runout compensation scheme is presented in section III along with simulation results. The robustness of the closed-loop system to variation in plant parameters is mathematically established in section IV. Simulation results presented in this section indicate that large variation in parameters can be tolerated. Experimental results are presented in section V. These results verify that asymptotic stability of the plant and sensor runout compensation remain unaffected by significant variation in plant parameters.

II. MODEL OF MAGNETIC BEARING WITH SENSOR RUNOUT

Consider the magnetically levitated rigid rotor in Fig.1. The rotor has two degrees of freedom along the x and y axes; the displacements along these axes are measured by non-contact gap sensors. The dynamics of the rotor along these axes, which are both inclined at 45° with the horizontal, are decoupled but similar. Along the x axis, one may write

$$m\ddot{x} = F - m\bar{g}, \qquad \bar{g} \triangleq g/\sqrt{2} \tag{1}$$

where m is the mass of the rotor, x is the rotor position, F is the magnetic force, and g is the acceleration due to gravity. The magnetic force can be expressed as (Siegwart, 1992)

$$F = k\left[\left(\frac{i_{10}+I}{l-x}\right)^2 - \left(\frac{i_{20}-I}{l+x}\right)^2\right] \tag{2}$$

where k is the magnetic force constant, l is the nominal air gap, i_{10}, i_{20} are the bias currents in the top and bottom electromagnets, and I is the control current. By linearizing Eq.(2) about $x = 0$, $I = 0$, Eq.(1) can be written as

$$m\ddot{x} = K_s x + K_c I, \qquad K_s \triangleq 2k\left(i_{10}^2 + i_{20}^2\right)/l^3, \quad K_c \triangleq 2k\left(i_{10} + i_{20}\right)/l^2 \tag{3}$$

where K_s and K_c are the magnetic stiffness and actuator gain of the magnetic bearing, respectively. The true location of the rotor geometric center is not available for a magnetic bearing with sensor runout. Instead, the gap sensors provide the signal x_s

$$x_s = x + d \tag{4}$$

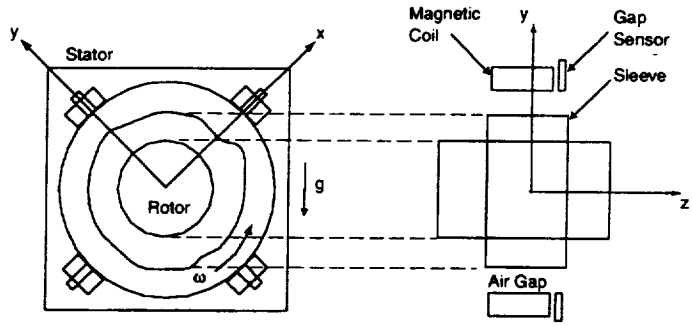

Figure 1. A magnetic bearing system with sensor runout.

where, d, the sensor runout disturbance, can be expressed by the Fourier series

$$d = a_0 + \sum_{i=1}^{n} a_i \sin(i\omega t) + b_i \cos(i\omega t) \tag{5}$$

In the above expression, ω is the rotor angular speed, n is the number of harmonics, a_0 is the DC component, and a_i, b_i, $i = 1, 2, \cdots, n$, are the harmonic Fourier coefficients. The effect of runout can be inferred from the block diagram of the magnetic bearing control system in Fig.2. Unless compensated, runout will seriously degrade performance of the system. Specifically, it will cause undesirable rotor vibration and may ultimately result in failure.

III. SENSOR RUNOUT COMPENSATION SCHEME

III-A. ADAPTIVE SENSOR RUNOUT COMPENSATION (ASRC)

We present an adaptive controller for stabilization of the rotor geometric center to the origin through estimation and feedforward cancellation of sensor runout. We propose the controller to have the structure shown in Fig.2, where $\bar{x}$ is the estimated rotor geometric center, and $\bar{d}$ is the estimated sensor runout, defined as

$$\bar{x} = x_s - \bar{d}, \qquad \bar{d} \triangleq \bar{a}_0 + \sum_{i=1}^{n} \bar{a}_i \sin(i\omega t) + \bar{b}_i \cos(i\omega t) \tag{6}$$

In the above expression, $\bar{a}_0$ is the estimated value of a_0, and $\bar{a}_i$, $\bar{b}_i$ are estimated values of a_i, b_i, respectively, for $i = 1, 2, \cdots, n$. Using Eqs.(4) and (6), $\bar{x}$ can also be expressed as

$$\bar{x} = x + \tilde{d} \tag{7}$$

where, $\tilde{d}$, the error in the estimate of sensor runout disturbance, is given by the relation

$$\tilde{d} \triangleq (d - \bar{d}) = \boldsymbol{Y}^T \tilde{\boldsymbol{\phi}} \tag{8}$$

The regressor vector $\boldsymbol{Y}$, and the vector of parameter estimation errors $\tilde{\boldsymbol{\phi}}$, are defined as follows

$$\boldsymbol{Y} \triangleq [1 \quad \sin(\omega t) \quad \cos(\omega t) \quad \sin(2\omega t) \quad \cos(2\omega t) \quad \cdots \quad \cdots \quad \sin(n\omega t) \quad \cos(n\omega t)]^T \tag{9}$$

$$\tilde{\boldsymbol{\phi}} \triangleq [\tilde{a}_0 \quad \tilde{a}_1 \quad \tilde{b}_1 \quad \tilde{a}_2 \quad \tilde{b}_2 \quad \cdots \quad \cdots \quad \tilde{a}_n \quad \tilde{b}_n]^T \tag{10}$$

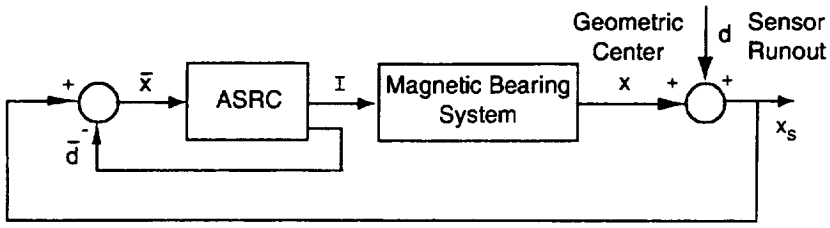

Figure 2. Block diagram of magnetic bearing system with sensor runout.

where $\tilde{a}_0 \triangleq (a_0 - \bar{a}_0)$, and $\tilde{a}_i \triangleq (a_i - \bar{a}_i)$, $\tilde{b}_i \triangleq (b_i - \bar{b}_i)$, $i = 1, 2, \cdots, n$. For estimation and cancellation of sensor runout, and stabilization of the rotor geometric center, we propose the control action

$$I = -\frac{1}{K_c}\left(K_s \bar{x} + m\lambda \dot{\bar{x}} + c\bar{e}\right), \qquad \bar{e} \triangleq (\dot{\bar{x}} + \lambda \bar{x}) \tag{11}$$

along with the adaptation law

$$\dot{\tilde{\phi}} = \boldsymbol{\Gamma} \boldsymbol{Y}_m \bar{e} \tag{12}$$

where $\boldsymbol{\Gamma} \in R^{(2n+1)\times(2n+1)}$ is a matrix of adaptation gains, $\boldsymbol{Y}_m$ is a regressor vector, defined as

$$\boldsymbol{\Gamma} \triangleq diag\,(\gamma_0, \gamma_1, \gamma_1, \gamma_2, \gamma_2, \cdots, \cdots, \gamma_n, \gamma_n), \qquad \boldsymbol{Y}_m \triangleq K_s \boldsymbol{Y} - m\dot{\boldsymbol{Y}} \tag{13}$$

and c, λ, and γ_i, $i = 0, 1, 2, \cdots, n$ are positive constants.

From the definition of $\boldsymbol{Y}$ and $\boldsymbol{Y}_m$ in Eqs.(9) and (13), we can establish

$$\dot{\boldsymbol{Y}}^T \boldsymbol{\Gamma} \boldsymbol{Y}_m = 0, \qquad \boldsymbol{Y}^T \boldsymbol{\Gamma} \dot{\boldsymbol{Y}}_m = 0 \tag{14}$$

Also, we define

$$\Delta \triangleq \boldsymbol{Y}^T \boldsymbol{\Gamma} \boldsymbol{Y}_m = \sum_{i=0}^{n} \gamma_i \left(K_s + m i^2 \omega^2\right) \tag{15}$$

and choose adaptation gains $\gamma_0, \gamma_1, \cdots, \gamma_n$ to guarantee $0 < \Delta < 1$. Substituting Eq.(11) into Eq.(3), the dynamics of the controlled rotor can be described by

$$m\ddot{x} = -K_s \tilde{d} - m\lambda \dot{\tilde{x}} - c\bar{e}$$

Using the relation $\ddot{\tilde{x}} = \ddot{x} + \ddot{\tilde{d}}$ from Eq.(7), and $\dot{\bar{e}} = \ddot{\tilde{x}} + \lambda \dot{\tilde{x}}$ from Eq.(11), the above equation can be rewritten as

$$m\dot{\bar{e}} = m\ddot{\tilde{d}} - K_s \tilde{d} - c\bar{e}$$

Substituting Eq.(8) and then using the relations in Eq.(14) and (15), we get

$$m(1 - \Delta)\dot{\bar{e}} = -\boldsymbol{Y}_m^T \tilde{\boldsymbol{\phi}} - c\bar{e}$$

The closed loop system dynamics can now be described by

$$\dot{\tilde{x}} = -\lambda \tilde{x} + \bar{e} \tag{16a}$$

$$\dot{\bar{e}} = -\frac{1}{m(1 - \Delta)}\left(\boldsymbol{Y}_m^T \tilde{\boldsymbol{\phi}} + c\bar{e}\right) \tag{16b}$$

$$\dot{\tilde{\boldsymbol{\phi}}} = \boldsymbol{\Gamma} \boldsymbol{Y}_m \bar{e} \tag{16c}$$

The following observations can now be made with respect to the closed-loop system.

Theorem 1:

Consider the sub-system described by Eqs.(16b) and (16c). For this system, $(\bar{e}, \widetilde{\phi}) \equiv (0,0)$ is an asymptotically stable equilibrium.

Proof: From Eqs.(16b) and (16c) first notice that $(\bar{e}, \widetilde{\phi}) = (0,0)$ implies $(\dot{\bar{e}}, \dot{\widetilde{\phi}}) = (0,0)$. Therefore, $(\bar{e}, \widetilde{\phi}) \equiv (0,0)$ is an equilibrium point. To show that this equilibrium is asymptotically stable, we define the continuously differentiable, positive definite function

$$V(\bar{e}, \widetilde{\phi}) = \frac{1}{2} m (1-\Delta) \bar{e}^2 + \frac{1}{2} \widetilde{\phi}^T \Gamma^{-1} \widetilde{\phi}, \qquad 0 < \Delta < 1 \tag{17}$$

The derivative of V can be computed as

$$\dot{V} = m (1-\Delta) \bar{e} \dot{\bar{e}} + \widetilde{\phi}^T \Gamma^{-1} \dot{\widetilde{\phi}}$$

Using Eqs.(16b) and (16c), we get

$$\dot{V} = -c\bar{e}^2 \leq 0 \tag{18}$$

Since V is positive definite and $\dot{V}$ is negative semi-definite, we conclude $(\bar{e}, \widetilde{\phi}) \equiv (0,0)$ is stable. In addition, since $\dot{V}$ is uniformly continuous, we use Barbalat's lemma (Khalil, 1996) to deduce $\dot{V} \to 0$ as $t \to \infty$. This implies $\bar{e} \to 0$ as $t \to \infty$. By differentiating Eq.(16b), we can show that $\ddot{\bar{e}} = \ddot{\bar{e}}(t, \widetilde{\phi}, \bar{e})$ is bounded. This implies that $\dot{\bar{e}}$ is uniformly continuous. Since $\bar{e} \to 0$ as $t \to \infty$, we once again use Barbalat's lemma (Khalil, 1996) to deduce $\dot{\bar{e}} \to 0$ as $t \to \infty$. Knowing $\bar{e}, \dot{\bar{e}} \to 0$ as $t \to \infty$, we can conclude from Eq.(16b)

$$\boldsymbol{Y}_m^T \widetilde{\phi} \to 0 \tag{19}$$

It can be shown that there exist positive constants α_1, α_2, and δ, such that

$$\alpha_2 \boldsymbol{I} \geq \int_t^{t+\delta} \boldsymbol{Y}_m \boldsymbol{Y}_m^T d\tau \geq \alpha_1 \boldsymbol{I}$$

where $\boldsymbol{I}$ is the identity matrix. Therefore $\boldsymbol{Y}_m$ is a persistently exciting signal (Khalil, 1996). This implies from Eq.(19) that $\widetilde{\phi} \to 0$, as $t \to \infty$. Knowing $\bar{e}, \widetilde{\phi} \to 0$, as $t \to \infty$, we can now assert that $(\bar{e}, \widetilde{\phi}) \equiv (0,0)$ is an asymptotically stable equilibrium. This concludes our proof.

Lemma 1:

The origin of the closed-loop system in Eq.(16), $(\bar{x}, \bar{e}, \widetilde{\phi}) \equiv (0,0,0)$, is an asymptotically stable equilibrium point.

Proof: The closed loop system in Eq.(16) is an interconnected system of the form

$$\dot{z}_1 = f_1(t, z_1, z_2) \tag{20a}$$

$$\dot{z}_2 = f_2(t, z_2) \tag{20b}$$

where $z_1 \triangleq \bar{x}$, and $z_2 \triangleq \begin{pmatrix} \bar{e} & \widetilde{\phi}^T \end{pmatrix}^T$ are the state variables of the two sub-systems. We know from Theorem 1 that $z_2 = 0$ is an asymptotically stable equilibrium of the sub-system in Eq.(20b). Also, $\dot{z}_1 = f_2(t, z_1, 0)$ has an asymptotically stable equilibrium point at $z_1 = 0$. This can be readily established from Eqs.(20b) and (16c). Using the asymptotic stability theorem for cascaded systems (Khalil, 1996), we conclude $(\bar{x}, \bar{e}, \widetilde{\phi}) \equiv (0,0,0)$, is an asymptotically stable equilibrium.

Theorem 2:

The coordinate $(x, \dot{x}, \tilde{\phi}) \equiv (0,0,0)$ is a stable equilibrium point for the closed loop system defined by Eqs.(3), (11), and (12).

Proof: Using Eqs.(7), (8), (11), (12), and (15), we can show that at $(x, \dot{x}, \tilde{\phi}) \equiv (0,0,0)$, we have

$$\tilde{d} = \boldsymbol{Y}^T \tilde{\boldsymbol{\phi}} = 0, \qquad \bar{x} = x + \tilde{d} = 0, \qquad \dot{\tilde{d}} = (\dot{\boldsymbol{Y}}^T \tilde{\boldsymbol{\phi}} + \boldsymbol{Y}^T \dot{\tilde{\boldsymbol{\phi}}}) = \boldsymbol{Y}^T \boldsymbol{\Gamma} \boldsymbol{Y}_m \bar{e} = \Delta \bar{e} = \Delta(\dot{\bar{x}} + \lambda \bar{x}) = \Delta \dot{\bar{x}}$$

Also, at $(x, \dot{x}, \tilde{\phi}) \equiv (0,0,0)$, $\dot{\tilde{d}} = (\dot{\bar{x}} - \dot{x}) = \dot{\bar{x}}$. Comparing with the expression for $\dot{\tilde{d}}$ above, we have $\dot{\bar{x}} = \dot{\bar{x}} = 0$, since $\Delta \neq 1$. From Eqs.(3), (11), and (12), it follows that $(\dot{x}, \ddot{x}, \dot{\tilde{\phi}}) = (0,0,0)$. Therefore, $(x, \dot{x}, \tilde{\phi}) \equiv (0,0,0)$ is an equilibrium point. The fact that $(x, \dot{x}, \tilde{\phi}) \equiv (0,0,0)$ is asymptotically stable can now be deduced from

(a) $(\bar{x}, \bar{e}, \tilde{\phi}) \equiv (0,0,0)$ is an asymptotically stable equilibrium (follows from Lemma 1),

(b) the transformation matrix $\boldsymbol{P}$ that maps $(\bar{x}, \bar{e}, \tilde{\phi})$ to $(x, \dot{x}, \tilde{\phi})$

$$\begin{pmatrix} x \\ \dot{x} \\ \tilde{\phi} \end{pmatrix} = \begin{pmatrix} & \boldsymbol{P} & \end{pmatrix} \begin{pmatrix} \bar{x} \\ \bar{e} \\ \tilde{\phi} \end{pmatrix}, \qquad \boldsymbol{P} \triangleq \begin{pmatrix} 1 & 0 & -\boldsymbol{Y}^T \\ -\lambda & (1-\Delta) & -\dot{\boldsymbol{Y}}^T \\ 0 & 0 & \boldsymbol{E} \end{pmatrix}$$

where $\boldsymbol{E} \in R^{(2n+1)\times(2n+1)}$ is the identity matrix, is well defined and upper bounded, and

(c) the inverse transformation $\boldsymbol{P}^{-1}$ exists, and $\| \boldsymbol{P}^{-1} \|$ is also upper bounded.

Theorem 2 establishes that the adaptive controller proposed herein guarantees stabilization of the rotor geometric center through identification and cancellation of sensor runout disturbance.

III-B. SIMULATION RESULTS

Simulation results are presented here to demonstrate effectiveness of the adaptive controller, discussed in the previous section. Though the controller was designed using a linearized model of the plant, we use the nonlinear plant model to simulate the real situation. The bearing parameters, which include rotor mass, magnetic force constant, nominal air gap, bias currents, magnetic stiffness, and actuator gain, were assumed to be the ones in our experimental hardware. These values can be referenced from table 1 in section V. The Fourier coefficients of sensor runout disturbance were assumed to be $a_0 = 10$, $a_1 = 67.615$, $b_1 = 18.117$, $a_2 = 7.071$, $b_2 = 7.071$

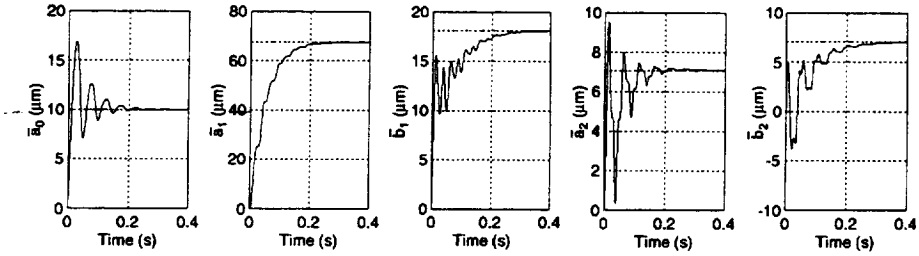

Figure 3. Estimated parameters of sensor runout; true values are shown with dashed lines.

where the units are in micrometers. Higher harmonics of the disturbance were assumed absent. The rotor initial conditions were assumed to be $x(0) = -1.0 \times 10^{-4}$ and $\dot{x}(0) = 0.0$, respectively, in SI units. The angular velocity of the rotor was assumed to be 1200 rpm. The simulation results for

error gains $\lambda = 400\ s^{-1}$, and $c = 1200\ kg/s$, and adaptation gains $\Gamma = diag\ (1,2,2,1,1,0.5,0.5) \times 10^{-7}$ m/N, are shown in Figs.3 and 4. These figures indicate that estimation of runout is successfully completed within 0.3 secs, and the rotor geometric center is effectively stabilized to the origin.

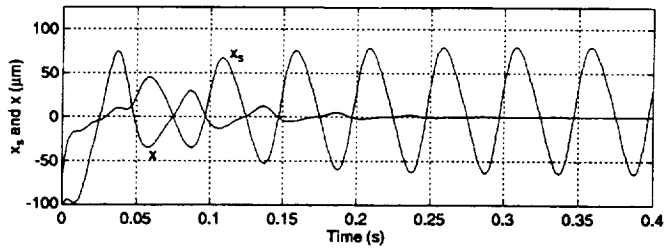

Figure 4. Stabilization of rotor geometric center in the presence of sensor runout.

IV. ROBUSTNESS TO UNCERTAIN PLANT PARAMETERS

IV-A. STRICT PASSIVITY OF CLOSED LOOP SYSTEM

In this section we establish that the adaptive sensor runout compensation (ASRC) scheme is robust to uncertainties and/or variation in plant parameters. Specifically, we show that ASRC guarantees stabilization of rotor geometric center and exact cancellation of sensor runout in the absence of exact knowledge of rotor mass, m, magnetic stiffness, K_s, and actuator gain, K_c. To this end, we estimate the values of these parameters to be $\bar{m}$, $\bar{K}_s$, and $\bar{K}_c$, respectively, and modify our control action and adaptation law in Eqs.(11) and (12), as follows

$$I = -\frac{1}{\bar{K}_c}\left(\bar{K}_s \bar{x} + \bar{m}\lambda \dot{\bar{x}} + c\bar{e}\right) \tag{21}$$

$$\dot{\tilde{\phi}} = \Gamma \bar{Y}_m \bar{e}, \qquad \bar{Y}_m \triangleq \bar{K}_s Y - \bar{m}\ddot{Y} \tag{22}$$

Substitution of Eq.(21) in Eq.(3) indicates that the closed-loop system takes the form

$$m\ddot{\bar{x}} + \frac{K_c}{\bar{K}_c}(\bar{m}\lambda + c)\dot{\bar{x}} + \left[\frac{K_c}{\bar{K}_c}(\bar{K}_s + c\lambda) - K_s\right]\bar{x} = m\ddot{\tilde{d}} - K_s\tilde{d} \tag{23}$$

Using Eqs.(8), (13) and (22), the right hand side of Eq.(23) can be simplified as follows

$$\begin{aligned} m\ddot{\tilde{d}} - K_s\tilde{d} &= m\left(\ddot{Y}^T\tilde{\phi} + 2\dot{Y}^T\dot{\tilde{\phi}} + Y^T\ddot{\tilde{\phi}}\right) - K_s Y^T\tilde{\phi} \\ &= -Y_m^T\tilde{\phi} + m\left[2\dot{Y}^T\Gamma\bar{Y}_m\bar{e} + Y^T\Gamma\left(\dot{\bar{Y}}_m\bar{e} + \bar{Y}_m\dot{\bar{e}}\right)\right] \end{aligned}$$

Using the identities $\dot{Y}^T\Gamma\bar{Y}_m = 0$, $Y^T\Gamma\dot{\bar{Y}}_m = 0$, we get

$$m\ddot{\tilde{d}} - K_s\tilde{d} = -Y_m^T\tilde{\phi} + m\bar{\Delta}\dot{\bar{e}}, \qquad \bar{\Delta} \triangleq Y^T\Gamma\bar{Y}_m = \sum_{i=0}^{n}\gamma_i\left(\bar{K}_s + \bar{m}i^2\omega^2\right) \tag{24}$$

Substituting Eq.(24) into Eq.(23), we get the closed-loop system dynamics

$$M\ddot{\bar{x}} + C\dot{\bar{x}} + K\bar{x} = -Y_m^T\tilde{\phi} \tag{25}$$

where M, C, and K, are defined as follows

$$M \triangleq m(1-\bar{\Delta}), \qquad C \triangleq \frac{K_c}{\bar{K}_c}(\bar{m}\lambda + c) - m\lambda\bar{\Delta}, \qquad K \triangleq \left[\frac{K_c}{\bar{K}_c}(\bar{K}_s + c\lambda) - K_s\right] \tag{26}$$

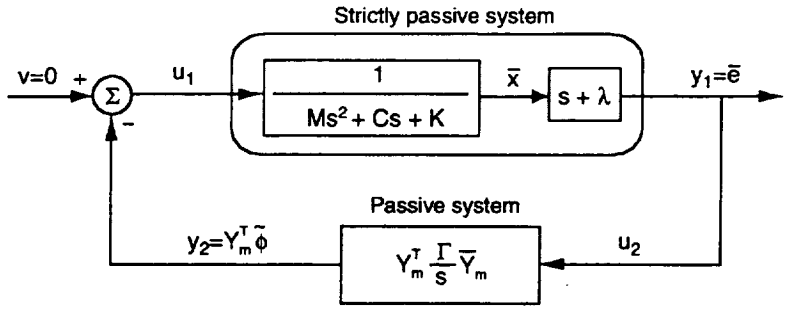

Figure 5. Block diagram of closed-loop system in the presence of uncertainty.

The closed loop system, described by the dynamics of the rotor in Eq.(25) and the adaptation law in Eq.(22) is represented by the block diagram in Fig.5, which is a feedback inter-connection of two linear systems. The following observations can be made regarding these linear systems.

Lemma 1: The linear system in the forward path in Fig.5, defined by the transfer function

$$G(s) = \frac{s+\lambda}{Ms^2 + Cs + K}$$

is strictly passive if $M, C, K > 0$, and $C - \lambda M > 0$.

Proof: If $M, C, K > 0$, G(s) is Hurwitz. Furthermore, if $C - \lambda M > 0$, we have

$$G(j\omega) + G(-j\omega) > 0, \qquad G(\infty) = 0, \qquad \lim_{\omega\to\infty} \omega^2 \left[G(j\omega) + G(-j\omega)\right] > 0$$

Therefore, $G(s)$ is strictly positive real (Khalil, 1996). The Kalman-Yakubovich-Popov lemma can now be used (Khalil, 1996) to show that $G(s)$ is strictly passive.

Lemma 2: The linear system in the feedback path of Fig.5 is passive.

Proof: The adaptation law in Eq.(22) can be written as

$$\dot{\tilde{a}}_0 = \gamma_0 \bar{K}_s \bar{e}, \qquad \dot{\tilde{a}}_i = \gamma_i \left[\bar{K}_s + \bar{m}i^2\omega^2\right] \sin(i\omega t)\,\bar{e}, \qquad \dot{\tilde{b}}_i = \gamma_i \left[\bar{K}_s + \bar{m}i^2\omega^2\right] \cos(i\omega t)\,\bar{e}, \qquad i = 1, 2, \cdots, n$$

Using these relations, and defining

$$\rho_i = \frac{K_s + mi^2\omega^2}{\gamma_i(\bar{K}_s + \bar{m}i^2\omega^2)}$$

for $i = 0, 1, 2, \cdots, n$, we can express the net energy flow into the system as

$$\begin{aligned}
\int_0^t y_2 u_2\, dt = \int_0^t \mathbf{Y}_m^T \tilde{\boldsymbol{\phi}}\, \bar{e}\, dt &= K_s \int_0^t \tilde{a}_0 \bar{e}\, dt + \sum_{i=1}^{n} (K_s + mi^2\omega^2) \int_0^t \left[\tilde{a}_i \sin(i\omega t)\bar{e} + \tilde{b}_i \cos(i\omega t)\bar{e}\right] dt \\
&= \rho_0 \int_0^t \tilde{a}_0 \dot{\tilde{a}}_0\, dt + \sum_{i=1}^{n} \rho_i \int_0^t \left[\tilde{a}_i \dot{\tilde{a}}_i + \tilde{b}_i \dot{\tilde{b}}_i\right] dt \\
&= \frac{\rho_0}{2}\left[\tilde{a}_0^2(t) - \tilde{a}_0^2(0)\right] + \sum_{i=1}^{n} \frac{\rho_i}{2}\left[\tilde{a}_i^2(t) + \tilde{b}_i^2(t) - \tilde{a}_i^2(0) - \tilde{b}_i^2(0)\right] \\
&= W[\tilde{\boldsymbol{\phi}}(t)] - W[\tilde{\boldsymbol{\phi}}(0)]
\end{aligned} \tag{27}$$

where $W[\tilde{\phi}(t)]$ is a positive definite energy storage function given by the relation

$$W[\tilde{\phi}(t)] \triangleq \frac{1}{2}\tilde{\phi}^T M \tilde{\phi}, \qquad M \triangleq diag\,(\rho_0, \rho_1, \rho_1, \rho_2, \rho_2, \cdots, \cdots, \rho_n, \rho_n)$$

From Eq.(27) we claim passivity (Khalil, 1996).

We now present our final result with the help of the following theorem.

Theorem 3: (Asymptotic stability and robustness)

The control and adaptation laws in Eqs.(21) and (22) guarantee asymptotic stability of the equilibrium $(x, \dot{x}, \tilde{\phi}) \equiv (0,0,0)$ of the magnetic bearing system in Eq.(3) in the presence of uncertainty in rotor mass, m, magnetic stiffness, K_s, and actuator gain, K_c, provided the error and adaptation gains are chosen to satisfy $M, C, K > 0$, and $C - \lambda M > 0$.

Proof: Through proper choice of the error gains c, λ, and adaptation gains γ_i, $i = 0, 1, 2, \cdots, n$, we can easily guarantee $M, C, K > 0$, and $C - \lambda M > 0$. Using Lemmas 1 and 2, we can then conclude that the closed-loop system is a feedback interconnection of a strictly passive system and a passive system. Using the passivity theorem from the appendix (Krstic, et al., 1995) we claim $(\bar{x}, \dot{\bar{x}}, \tilde{\phi}) \equiv (0,0,0)$ is globally uniformly stable, and $\bar{x}, \dot{\bar{x}} \to 0$ as $t \to \infty$.

Now, to show $(x, \dot{x}, \tilde{\phi}) \equiv (0,0,0)$ is an asymptotically stable equilibrium, we first need to show that $(x, \dot{x}, \tilde{\phi}) \equiv (0,0,0)$ is an equilibrium. This can be verified using Eqs.(3), (8), (21), and (22), and is left to the reader. The fact that $(x, \dot{x}, \tilde{\phi}) \equiv (0,0,0)$ is stable follows from
(a) $(\bar{x}, \dot{\bar{x}}, \tilde{\phi}) \equiv (0,0,0)$ is globally uniformly stable,
(b) the transformation matrix $\boldsymbol{P}(t)$ that maps $(\bar{x}, \dot{\bar{x}}, \tilde{\phi})$ to $(x, \dot{x}, \tilde{\phi})$ is well defined and $\| \boldsymbol{P} \|$ is upper bounded, and
(c) the inverse transformation $\boldsymbol{P}^{-1}$ exists, and $\| \boldsymbol{P}^{-1} \|$ is also upper bounded.
Finally, we prove $(x, \dot{x}, \tilde{\phi}) \to (0,0,0)$ as $t \to \infty$. Since $\bar{x}, \dot{\bar{x}} \to 0$, $\bar{e} \to 0$. Also, from Fig.5 we claim $u_1 = y_2 \to 0$. This is true since the mass-spring-damper system in Fig.5 cannot have zero output for nonzero input. Since $\boldsymbol{Y}_m^T$ is persistently exciting, as discussed in the proof of theorem 1, $y_2 = 0$ implies $\tilde{\phi} = 0$, and $\tilde{d} = \boldsymbol{Y}^T \tilde{\phi} = 0$. Also, $\dot{\tilde{d}} = (\dot{\boldsymbol{Y}}^T \tilde{\phi} + \boldsymbol{Y}^T \dot{\tilde{\phi}}) = \boldsymbol{Y}^T \dot{\tilde{\phi}} = \boldsymbol{Y}^T \boldsymbol{\Gamma} \boldsymbol{Y}_m \bar{e} = 0$. We conclude the proof by simply showing $x \triangleq (\bar{x} - \tilde{d}) \to 0$ and $\dot{x} \triangleq (\dot{\bar{x}} - \dot{\tilde{d}}) \to 0$.

IV-B. SIMULATION RESULTS

To demonstrate robustness of the adaptive controller to parameter uncertainties, we present simulation results using the nonlinear model of our magnetic bearing. The nominal parameter values were assumed to be the ones in our experimental hardware; these values can be referenced from table 1 in section V. The nominal values, along with the error and adaptation gains, satisfy the asymptotic stability conditions in theorem 3, namely

$$M = 1.94 > 0, \quad C = 1.97 \times 10^3 > 0, \quad K = 4.8 \times 10^5 > 0, \quad (C - \lambda M) = 1.2 \times 10^3 > 0 \qquad (28)$$

The above values in SI units, which were computed from the expressions in Eq.(26), support the simulation results in Figs.3 and 4. To demonstrate robustness, we over-estimate the uncertain parameters, namely, rotor mass, magnetic stiffness, and actuator gain, by 100%. The Fourier coefficients of sensor runout, rotor initial conditions, angular velocity, error gains, and adaptation

gains were chosen as in section III-B. The results in Figs.6 and 7 indicate sensor runout is exactly estimated and the rotor geometric center is successfully stabilized to the origin. These results can be independently asserted from the conditions for asymptotic stability in theorem 3, namely

$$M = 1.44 > 0, \quad C = 1.18 \times 10^3 > 0, \quad K = 2.4 \times 10^5 > 0, \quad (C - \lambda M) = 0.6 \times 10^3 > 0 \qquad (29)$$

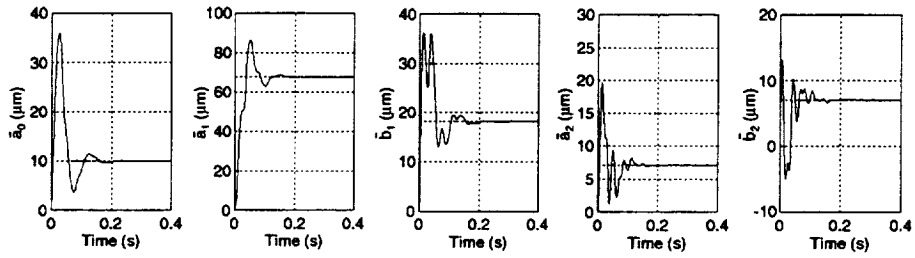

Figure 6. Sensor runout estimation for uncertain plant; true values shown in dashed lines.

A comparison of Figs.3 and 6 and Figs.4 and 7 indicates that the closed-loop system with 100% over-estimated parameters has better transient response than the closed-loop system with known parameters. This only indicates that the same set of error gains and adaptation gains will not necessarily result in the same performance of different systems. It is obvious from the values of M, C, K in Eqs.(28) and (29) that parameter uncertainty changes the forward path transfer function in Fig.5. The time-varying feedback in Fig.5 also changes due to uncertainty.

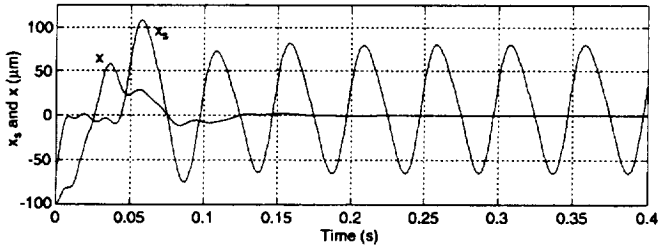

Figure 7. Stabilization of rotor for uncertain plant in the presence of sensor runout.

V. EXPERIMENTAL RESULTS

In this section we present experimental data to validate the theoretical results presented in sections III and IV. The parameters of the bearing and rotor assembly are as follows:

Table 1. Magnetic Bearing Test Rig Parameters

Parameter	Value
rotor mass, m	2.43 kg
electromagnetic force constant, k	2.82×10^{-6} Nm^2/A^2
nominal air gap, l	0.508×10^{-3} m
top coil bias current, I_{10}	2.41 A
bottom coil bias current, I_{20}	2.06 A
actuator gain, K_c	97.71 N/A
magnetic stiffness, K_s	4.33×10^5 N/m

The adaptive controller was implemented in Matlab/Simulink^{TM} environment and downloaded to a Digital Signal Processor (DSP) board, manufactured by DSpace. The DSP board, sampling approximately at 13 KHz, was used to control the rotor along both bearing axes, independently. The runout disturbance was assumed to be comprised of two harmonics in addition to the DC component. Under this computation load, the DSP allowed us to store ten signals, five per axis, in real time. For the x axis we stored the estimated position, $\bar{x}$, current, I_x, and the DC component and estimated Fourier coefficients of the first harmonic, $\bar{a}_{0x}$, $\bar{a}_{1x}$, $\bar{b}_{1x}$. The estimated coefficients of the second harmonic were found to be negligible but could not be stored due to DSP limitations. The sensor signal, x_s, was regenerated from stored data $\bar{x}$, $\bar{a}_{0x}$, $\bar{a}_{1x}$, and $\bar{b}_{1x}$, using Eq.(6). Since the second harmonic coefficients were used in the computation of $\bar{x}$, regeneration of x_s from $\bar{x}$ in the absence of these coefficients lacks some accuracy. Our choice of real-time signals for the y axis was exactly the same as that for the x axis.

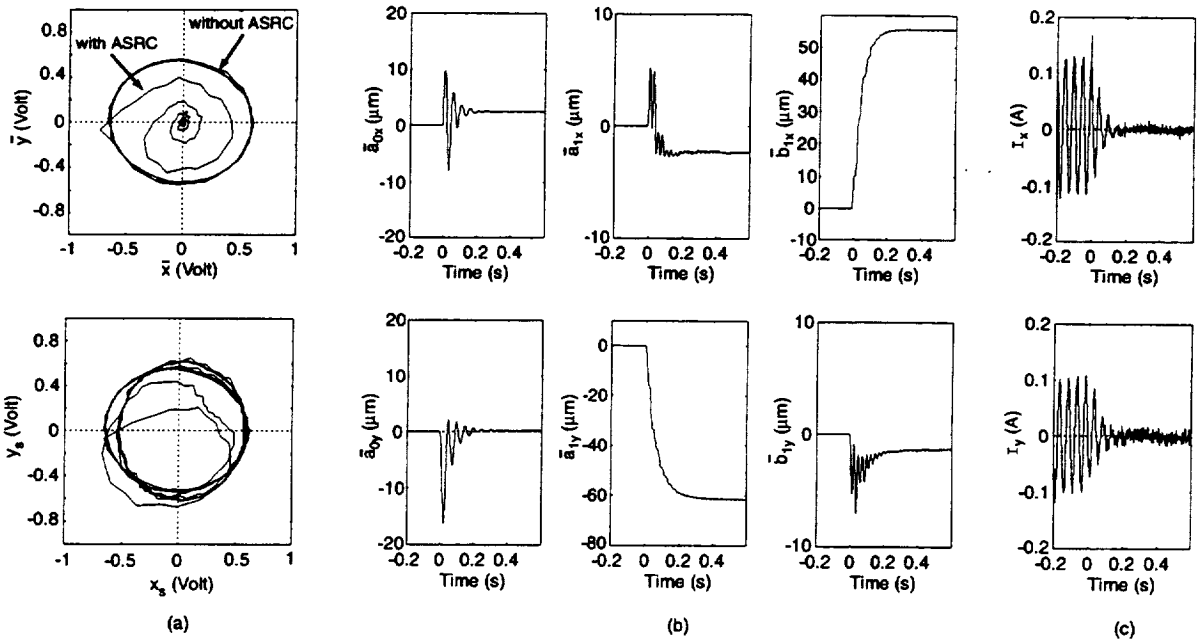

Figure 8. Trajectory of (a) estimated rotor geometric center and regenerated sensor signals, scale $1\ V = 50\ \mu m$ (b) estimated Fourier coefficients of sensor runout, and (c) control currents, with and without ASRC. The controller used known plant parameter values.

The electromagnets were driven by switching power amplifiers, product of Advanced Motion Control, operating with 1.6 KHz bandwidth. To ensure negligible effects due to unbalance, the rotor was well balanced and spun at the relatively low rpm of 1200. This speed is 20 times less than the first critical speed of the rotor, and guarantees negligible effects due to flexibility, which was not considered in our model. The error and adaptations gains of the adaptive controller, given by Eqs.(11) and (21), were chosen as

$$\lambda = 400\ s^{-1}, \qquad c = 1200\ kg/s, \qquad \Gamma = diag(1.0, 1.7, 1.7, 1.5, 1.5) \times 10^{-7}\ m/N \tag{30}$$

In controller implementation, the derivative of the estimated position signal, $\dot{\bar{x}}$, was numerically computed using the transfer function $2500s/(s + 2500)$. This eliminates potential problems arising from infiltration of wideband noise into the sensor signal.

Controller using known plant parameters We first present experimental results based on control and adaptation laws in Eqs.(11) and (12). In the control law, the values of m, K_s, and K_c were taken from Table 1. The trajectory of the estimated rotor geometric center $(\bar{x}, \bar{y})$ and regenerated trajectory of geometric center provided by the position sensors (x_s, y_s) are shown in Fig.8 (a). These trajectories indicate that while the sensors continue to provide geometric center positions corrupt with runout disturbance, their estimated values are stabilized to the origin with ASRC. It is seen from Fig.8 (b) that estimation of Fourier coefficients of runout are completed in 0.3 seconds. In the same time, sinusoidal variation in the control currents vanish in Fig.8 (c). These zero steady-state control currents imply stabilization of rotor geometric center to the origin in the absence of mass unbalance. Indeed, we can verify from Eq.(3) that the rotor would become unstable if this was not the case. We ensured negligible mass unbalance effects in our experiments through rotor balancing and by spinning the rotor at low rpm. Knowing that the rotor geometric center has stabilized to the origin, runout disturbance was obtained from the Fourier coefficients in Fig.8 (b). The trajectories of x_s, y_s in Fig.8 (a) also provide this information.

Controller using larger plant parameter values To demonstrate the robustness of ASRC to parameter uncertainty, we used control and adaptation laws in Eqs.(21) and (22). The parameter values $\bar{m}$, $\bar{K}_s$, and $\bar{K}_c$ in the control law were chosen to be 25% larger than the values of m, K_s, and K_c, respectively, provided in Table 1. The results obtained from our experiments are shown in Fig.9. These results indicate that runout is eliminated and the rotor geometric center is successfully stabilized to the origin despite error in the model used to construct the controller.

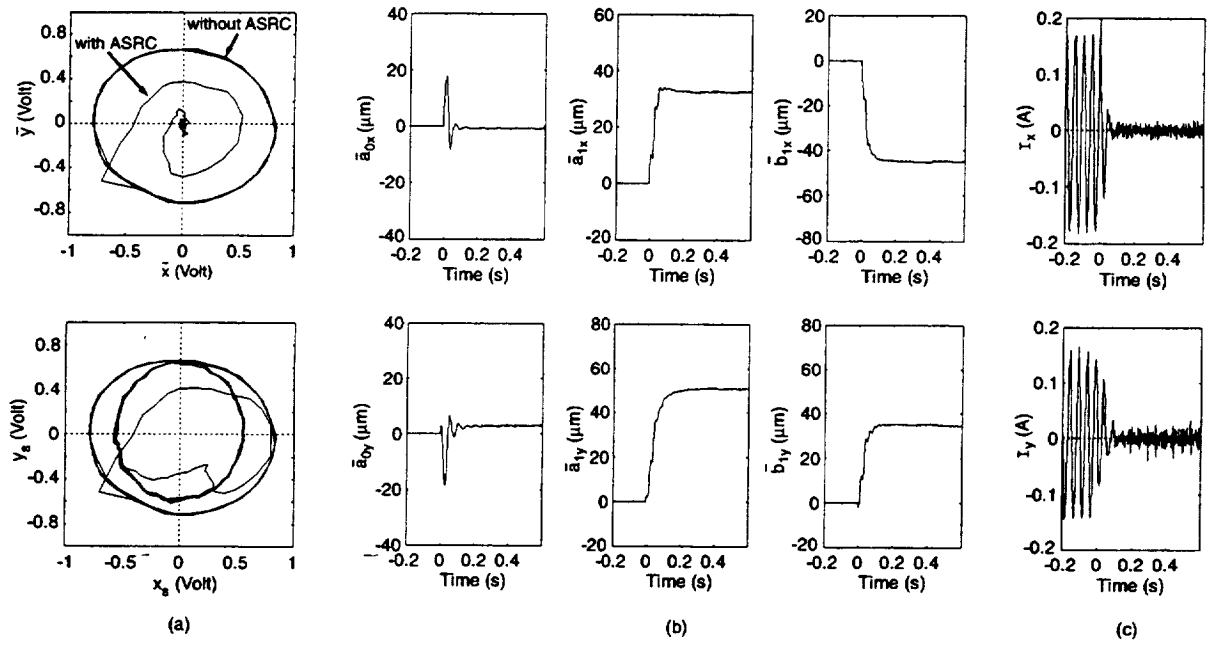

Figure 9. Trajectory of (a) estimated rotor geometric center and regenerated sensor signals, scale $1\ V = 50\ \mu m$, (b) estimated Fourier coefficients of sensor runout, and (c) control currents, with and without ASRC. To demonstrate robustness 25% larger parameter values were used.

VI. CONCLUSION

This paper presents a simple, yet robust, algorithm for adaptive compensation of sensor runout in active magnetic bearings. The algorithm is based on a rigid rotor model with no mass unbalance and assumes the angular speed of the rotor to be known and constant. Using powerful tools such as Lyapunov stability, persistency of excitation, and passivity, the algorithm is shown to guarantee perfect cancellation of runout harmonics and stabilization of the rotor geometric center. Through modeling, estimation, and cancellation of the DC component of runout, the algorithm generates the equivalent action of integral feedback for elimination of steady state errors. The algorithm is also robust to significant variation in plant parameters that include rotor mass, magnetic stiffness, and actuator gain. The effectiveness of our algorithm is validated through numerical simulations, as well as experiments. We present experimental data that confirm stabilization of the geometric center of a rotor with negligible mass unbalance effects, even when the modelled plant parameters are quite different. As compared to existing results on compensation of periodic disturbances, our algorithm has the combined advantages of simplicity of design and implementation, closed-loop estimation and cancellation of disturbances, stability of the overall system, and importantly, robustness to parameter variation. Our algorithm can also be used for compensation of mass unbalance, but in such applications the rotor will be stabilized about its inertial center. Our future work will address the important problem of combined mass unbalance and sensor runout compensation with rotor stabilization about the geometric center.

ACKNOWLEDGEMENT

The authors thank Dr. Hassan Khalil for his useful comments and suggestions.

REFERENCES

[1] Batty, R., 1988, "Notch filter control of magnetic bearings", MS Thesis, Massachussetts Institute of Technology, Cambridge, MA.

[2] Bleuler, H., Gahler, C., Herzog, R., Larsonneur, R., Mizuno, T., Siegwart, R., and Woo, S. -J., 1994, "Application of digital signal processors for industrial magnetic bearings", IEEE Transactions on Control Systems Technology, Vol.2, No.4, pp.280-289.

[3] Chen, D., and Paden, B., 1993, "Adaptive linearization of hybrid step motors: Stability analysis", IEEE Transactions on Automatic Control, Vol.38, No.6, pp.874-887.

[4] Fujita, M., Hatake, K., and Matsumura, F., 1993, "Loop shaping based robust control of a magnetic bearing", IEEE Control Systems, pp.57-65.

[5] Herzog, R., Buhler, P., Gahler, C., and Larsonneur, R., 1996, "Unbalance Compensation using generalized notch filters in multivariable feedback of magnetic bearings", IEEE Transactions on Control Systems Technology, Vol.4, No.5, pp.580-586.

[6] Hisatani, M., and Koizumi, T., 1994, "Adaptive filtering for unbalance vibration suppression", 4th ISMB, ETH Zurich, Switzerland.

[7] Hu, J., and Tomizuka, M., 1993, "A new plug-in adaptive controller for rejection of periodic disturbances", ASME J. of Dyn. Sys., Meas., and Cont., 115, pp.543-546.

[8] Khalil, H., 1996, "Nonlinear Systems", 2nd Ed., Prentice Hall, Upper Saddle River, NJ 07458.

[9] Kim, C. -S., and Lee, C. -W., "In situ runout identification in active magnetic bearing system by extended influence coefficient method", IEEE/ASME Trans. on Mechatronics, 2(1), pp.51-57.

[10] Knospe, C. R., 1991, "Stability and performance of notch filters for unbalance response", Proc. ISMST, NASA Langley Research Center, Hampton, VA.

[11] Knospe, C. R., Hope, R. W., Tamer, S. M., and Fedigan, S. J., 1996, "Robustness of adaptive unbalance control of rotors with magnetic bearings", J. of Vibration and Control, 2, pp.33-52.

[12] Knospe, C. R., Tamer, S. M., and Fedigan, S. J., 1997, "Robustness of adaptive rotor vibration control to structured uncertainty", ASME JDSMC, 119, pp.243-250.

[13] Krstic, M., Kanellakopoulos, I., and Kokotovic, P., 1995, "Nonlinear and adaptive control design", Wiley Interscience, New York, NY.

[14] Lum, K. -Y., Coppola, V., and Bernstein, D., 1996, "Adaptive autocentering control for an active magnetic bearing supporting a rotor with unknown mass imbalance", IEEE Transactions on Control Systems Technology, Vol.4, No.5, pp.587-597.

[15] Matsumura, F., Fujita, M., and Okawa, K., 1990, "Modeling and control of magnetic bearing systems achieving a rotation around the axis of inertia", 2nd ISMB, Tokyo, Japan, pp.273-280.

[16] Mizuno, T., and Higuchi, T., 1990, "Design of magnetic bearing controllers based on disturbance estimation", Proc. 2nd Int. Symp. on Magnetic Bearings, Tokyo, Japan, pp.281-288.

[17] Mohamed A. M., Matsumura, M., Namerikawa, T., and Lee, J., 1997, "Q-parameterization control of vibrations in a variable speed magnetic bearing", Proc. 1997 IEEE Int. Conf. on Control Applications, Hartford, CT.

[18] Na, H. -S., and Park, Y., 1997, "An adaptive feedforward controller for rejection of periodic disturbances", Journal of Sound and Vibration, 201(4), pp.427-435.

[19] Narendra, K. S., and Annaswamy, A. M., 1989, "Stable adaptive systems", Prentice Hall, Englewood Cliffs, NJ 07632.

[20] Paul, M., Hoffman, W., and Steffani, H. F., 1998, "Compensation for unbalances with aid of neural networks", 6th ISMB, Cambridge, MA.

[21] Reining, K. D., and Desrochers, A. A., 1986, "Disturbance accomodating controllers for rotating mechanical systems", ASME J. of Dyn. Sys., Meas., and Cont., 108, pp.24-31.

[22] Rutland, N. K., Keogh, P. S., and Burrows, C. R., 1994, "Comparison of controller designs for attenuation of vibration in a rotor bearing system under synchronous and transient conditions", 4th ISMB, ETH Zurich, Switzerland, pp.107-112.

[23] Sacks, A., Bodson, M., and Khosla, P., "Experimental results of adaptive periodic disturbance cancellation in a high performance magnetic disk drive", ASME JDSMC, 118, pp.416-424.

[24] Setiawan, J. D., Mukherjee, R., Maslen, E. H., and Song, G., 1999, "Adaptive compensation of sensor runout and mass unbalance in magnetic bearing systems", Proc. IEEE/ASME Int. Conf. on Advanced Intelligent Mechatronics, Atlanta, GA, September 1999.

[25] Shafai, B., Beale, S., Larocca, P., and Cusson, E., 1994, "Magnetic bearing control systems and adaptive forced balancing", IEEE Control Systems, 14, pp.4-13.

[26] Siegwart, R., 1992, "Design and applications of active magnetic bearings for vibration control", Von Karman Inst. Fluid Dyn. Lec. Series 1992-06, Vibration and Rotor Dynamics.

[27] Song, G., and Mukherjee, R., 1996, "Integrated adaptive robust control of active magnetic bearings", IEEE Int. Conf. on System, Man, and Cybernetics, Beijing, China.